

# Dilepton Production from Parton Interactions in the Early Stage of Relativistic Heavy-Ion Collisions

O. Linnyk<sup>a</sup>, E. L. Bratkovskaya<sup>a</sup>, J. Manninen<sup>b</sup>, and W. Cassing<sup>b</sup>

<sup>a</sup>Institut für Theoretische Physik, Universität Frankfurt, 60438 Frankfurt am Main, Germany

<sup>b</sup>Institut für Theoretische Physik, Universität Giessen, 35392 Giessen, Germany

E-mail: linnyk@fias.uni-frankfurt.de

**Abstract.** We address the dilepton production from the parton interactions in the early stage of relativistic heavy-ion collisions within the parton-hadron-string dynamics (PHSD) off-shell transport approach. The description of partons in PHSD is based on the dynamical quasiparticle model (DQPM) matched to reproduce lattice QCD results in thermodynamic equilibrium. According to the DQPM the constituents of the strongly interacting quark-gluon plasma (sQGP) are massive and off-shell quasi-particles (quarks and gluons) with broad spectral functions. In order to address the electromagnetic radiation of the sQGP, we derive off-shell cross sections of  $q\bar{q} \rightarrow \gamma^*$ ,  $q\bar{q} \rightarrow \gamma^* + g$  and  $qg \rightarrow \gamma^*q$  ( $\bar{q}g \rightarrow \gamma^*\bar{q}$ ) reactions taking into account the effective propagators for quarks and gluons from the DQPM. Dilepton production in In+In collisions at 158 AGeV and in Au+Au at  $\sqrt{s} = 200$  GeV is calculated by implementing these off-shell processes into the PHSD transport approach. By comparing to the data of the NA60 and PHENIX Collaborations, we study the relative importance of different dilepton production mechanisms and point out the regions in phase space where partonic channels are dominant.

Dileptons are emitted over the entire space-time evolution of the heavy-ion collision, from the initial nucleon-nucleon collisions through the hot and dense phase and to the hadron decays after the freeze-out. This is both a challenge and advantage of the probe. The separation of different “physics” in the dilepton radiation is nontrivial due to the non-equilibrium nature of the heavy-ion reactions, and covariant transport models have to be used to disentangle the various sources that contribute to the final dilepton spectra seen experimentally.

## 1. The PHSD approach to dilepton radiation

To address the dilepton production in a hot and dense medium – as created in heavy-ion collisions – we employ an up-to-date relativistic transport model, the Parton Hadron String Dynamics [1] (PHSD), that incorporates the explicit partonic phase in the early reaction region. Within PHSD, one solves generalized transport equations on the basis of the off-shell Kadanoff-Baym equations for Green’s functions in phase-space representation (in the first order gradient expansion beyond the quasiparticle approximation). The approach consistently describes the full evolution of a relativistic heavy-ion collision from the initial hard scatterings and string formation through the dynamical deconfinement phase transition to the quark-gluon plasma (QGP) as well as hadronization and to the subsequent interactions in the hadronic phase. In the hadronic sector PHSD is equivalent to the Hadron-String-Dynamics (HSD) transport approach [2, 3, 4] that has been used for the description of  $pA$  and  $AA$  collisions from SIS to RHIC energies. In particular, (P)HSD incorporates off-shell dynamics for vector mesons – according

to Refs. [5] – and a set of vector-meson spectral functions [6] that covers possible scenarios for their in-medium modification.

In the *off-shell* transport description, the hadron spectral functions change dynamically during the propagation through the medium and evolve towards the on-shell spectral function in the vacuum. As demonstrated in [6] the off-shell dynamics is important for resonances with a rather long lifetime in vacuum but strongly decreasing lifetime in the nuclear medium (especially  $\omega$  and  $\phi$  mesons) and also proves vital for the correct description of dilepton decays of  $\rho$  mesons with masses close to the two pion decay threshold.

Let us remind the off-shell transport equations (see [7] for details). One starts with a first order gradient expansion of the Wigner transformed Kadanoff-Baym equation using the following expression for the memory integrals

$$I_1^{><}(x_1, x_2) = - \int_{-\infty}^{\infty} d^D x' \Theta(t_1 - t') [\Sigma^{>}(x_1, x') - \Sigma^{<}(x_1, x')] G^{><}(x', x_2) \quad (1)$$

$$+ \int_{-\infty}^{\infty} d^D x' \Sigma^{><}(x_1, x') \Theta(t_2 - t') [G^{>}(x', x_2) - G^{<}(x', x_2)] \\ = - \int_{-\infty}^{\infty} d^D x' \Sigma^R(x_1, x') G^{><}(x', x_2) + \Sigma^{><}(x_1, x') G^A(x', x_2). \quad (2)$$

and arrives at a generalized transport equation [5, 8]:

$$\underbrace{2p^\mu \partial_\mu^x i \bar{G}^{><} - \{\bar{\Sigma}^\delta + Re \bar{\Sigma}^R, i \bar{G}^{><}\}}_{\{\bar{M}, i \bar{G}^{><}\}} - \{i \bar{\Sigma}^{><}, Re \bar{G}^R\} = i \bar{\Sigma}^{<} i \bar{G}^{>} - i \bar{\Sigma}^{>} i \bar{G}^{<} \quad (3)$$

$$\{i \bar{\Sigma}^{><}, Re \bar{G}^R\} = i \bar{\Sigma}^{<} i \bar{G}^{>} - i \bar{\Sigma}^{>} i \bar{G}^{<} \quad (4)$$

as well as a generalized mass-shell equation

$$\underbrace{[p^2 - m^2 - \bar{\Sigma}^\delta - Re \bar{\Sigma}^R]}_{\bar{M}} i \bar{G}^{><} = i \bar{\Sigma}^{><} Re \bar{G}^R + \frac{1}{4} \{i \bar{\Sigma}^{>}, i \bar{G}^{<}\} - \frac{1}{4} \{i \bar{\Sigma}^{<}, i \bar{G}^{>}\} \quad (5)$$

with the mass-function  $\bar{M}$ . In the transport equation (3) one recognizes on the l.h.s. the drift term  $p^\mu \partial_\mu^x i \bar{G}^{><}$ , as well as the Vlasov term with the local self-energy  $\bar{\Sigma}^\delta$  and the real part of the retarded self-energy  $Re \bar{\Sigma}^R$ . On the other hand the r.h.s. represents the collision term with its typical ‘gain and loss’ structure.

The mass-function for fermions is

$$M_F(p, x) = \Pi_0^2 - \vec{\Pi}^2 - m_h^{*2}, \quad (6)$$

with the effective mass and four-momentum given by

$$m_h^*(x, p) = m_h + U_h^S(x, p), \quad \Pi^\mu(x, p) = p^\mu - U_h^\mu(x, p), \quad (7)$$

where  $U_h^S(x, p)$  and  $U_h^\mu(x, p)$  denote the real part of the scalar and vector self-energies of the particle, respectively, and  $m_h$  stands for its the bare (vacuum) mass. After inserting (6) into the generalized transport equation (3), the covariant off-shell transport theory emerges, that has been denoted as HSD [2, 4]. It is formally written as a coupled set of transport equations for the phase-space distributions  $N_h(x, p)$  ( $x = (t, \vec{r})$ ,  $p = (\varepsilon, \vec{p})$ ) of fermion  $h$  [2, 4] with a spectral function  $A_h(x, p)$  (using  $i \bar{G}_h^{<}(x, p) = N_h(x, p) A_h(x, p)$ ), i.e. [9]

$$\left\{ \left( \Pi_\mu - \Pi_\nu \partial_\mu^p U_h^\nu - m_h^* \partial_\mu^p U_h^S \right) \partial_x^\mu + \left( \Pi_\nu \partial_\mu^x U_h^\nu + m_h^* \partial_\mu^x U_h^S \right) \partial_p^\mu \right\} N_h(x, p) A_h(x, p) \\ - \{i \bar{\Sigma}^{<}, Re \bar{G}^R\} = \sum_{h_2 h_3 h_4} Tr_2 Tr_3 Tr_4 [T^\dagger T]_{12 \rightarrow 34} \delta^4(\Pi + \Pi_2 - \Pi_3 - \Pi_4) \\ \times A_h(x, p) A_{h_2}(x, p_2) A_{h_3}(x, p_3) A_{h_4}(x, p_4) \quad (8)$$

$$\times \{N_{h_3}(x, p_3) N_{h_4}(x, p_4) \bar{f}_h(x, p) \bar{f}_{h_2}(x, p_2) - N_h(x, p) N_{h_2}(x, p_2) \bar{f}_{h_3}(x, p_3) \bar{f}_{h_4}(x, p_4)\}. \quad (9)$$

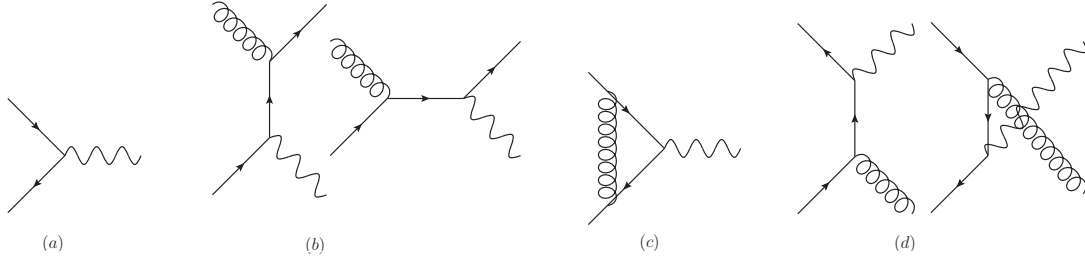


**Figure 1.** Diagrams contributing to the dilepton production from a QGP: (a) Born mechanism, (b) gluon-Compton scattering (GCS), (c) vertex correction, (d) gluon Bremsstrahlung (NLQDY), where virtual photons (wavy lines) split into lepton pairs; spiral lines denote gluons, arrows denote quarks. In each diagram the time runs from left to right.

Here  $\partial_\mu^x \equiv (\partial_t, \vec{\nabla}_r)$  and  $\partial_\mu^p \equiv (\partial_\varepsilon, \vec{\nabla}_p)$ , ( $\mu = 0, 1, 2, 3$ ). The backflow term in (8) is given by

$$- \{i\Sigma^<, ReG^R\} = \partial_p^\mu \left( \frac{M_h(x,p)}{M_h(x,p)^2 + \Gamma_h(x,p)^2/4} \right) \partial_\mu^x (N_h(x,p) \Gamma_h(x,p)) \quad (10)$$

$$- \partial_\mu^x \left( \frac{M_h(x,p)}{M_h(x,p)^2 + \Gamma_h(x,p)^2/4} \right) \partial_p^\mu (N_h(x,p) \Gamma_h(x,p)). \quad (11)$$

It stands for the off-shell evolution which vanishes in the on-shell limit, when the spectral function  $A_h(x,p)$  does not change its shape during the propagation through the medium, i.e.  $\vec{\nabla}_r \Gamma(x,p)=0$  and  $\vec{\nabla}_p \Gamma(x,p)=0$ . The set of coupled differential-integral equations (8) is solved using a test-particle ansatz.

The transport description of quarks and gluons in PHSD is based on the knowledge of the partonic propagators from a dynamical quasiparticle model for partons matched to reproduce lattice QCD results in thermodynamic equilibrium (DQPM). The DQPM describes QCD properties in terms of single-particle Green's functions (in the sense of a two-particle irreducible approach) and leads to the notion of the constituents of the sQGP being effective quasiparticles, which are massive and have broad spectral functions (due to large interaction rates). The transition from partonic to hadronic degrees of freedom in PHSD is described by covariant transition rates for the fusion of quark-antiquark pairs to mesonic resonances or three quarks (antiquarks) to baryonic states.

Dilepton radiation by the constituents of the QGP proceeds via the elementary processes illustrated in Fig. 1: the Born (Drell-Yan)  $q + \bar{q}$  annihilation mechanism, Gluon Compton scattering ( $q + g \rightarrow \gamma^* + q$  and  $\bar{q} + g \rightarrow \gamma^* + \bar{q}$ ), and quark + anti-quark annihilation with gluon Bremsstrahlung in the final state ( $q + \bar{q} \rightarrow g + \gamma^*$ ). In the on-shell approximation, one uses perturbative QCD cross sections for the processes listed above. However, in order to make quantitative predictions at experimentally relevant low dilepton mass and strong coupling, we have to take into account the non-perturbative spectral functions and self-energies of the quarks, anti-quarks and gluons thus going beyond the on-shell approximation. For this purpose, off-shell cross sections were derived in [10] for dilepton production in the reactions  $q + \bar{q} \rightarrow l^+ l^-$  (Drell-Yan mechanism),  $q + \bar{q} \rightarrow g + l^+ l^-$  (quark annihilation with the gluon Bremsstrahlung in the final state),  $q(\bar{q}) + g \rightarrow q(\bar{q}) + l^+ l^-$  (gluon Compton scattering),  $g \rightarrow q + \bar{q} + l^+ l^-$  and  $q(\bar{q}) \rightarrow q(\bar{q}) + g + l^+ l^-$  (virtual gluon decay, virtual quark decay) in the sQGP in effective perturbation theory by dressing the quark and gluon lines with the DQPM propagators for quarks and gluons. The obtained off-shell elementary cross sections then are implemented into the PHSD transport code, where the masses of quarks and gluons are distributed according to the DQPM spectral functions.

For illustration, we plot the dilepton production cross sections in the Born mechanism in

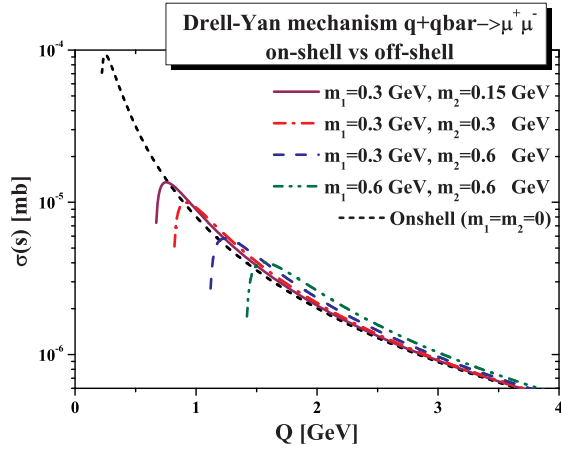


**Figure 2.** Dilepton production cross sections in the Born channel ( $q + \bar{q} \rightarrow \mu^+ + \mu^-$ ). The short dashed (black) line shows the on-shell, i.e. the standard pQCD result. The other lines show the off-shell cross section, in which the annihilating quark and antiquark have finite masses  $m_1$  and  $m_2$  with different values.

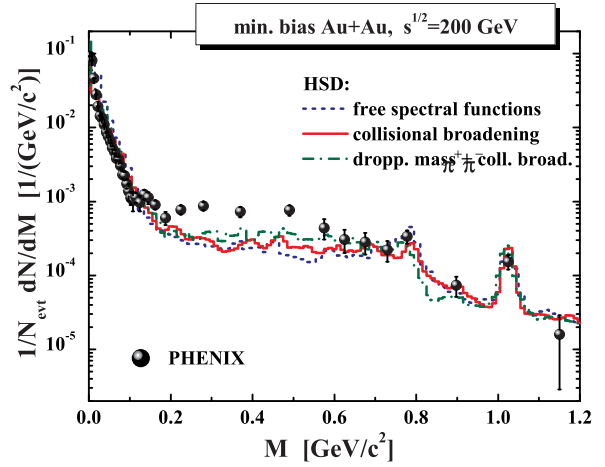


**Figure 3.** The HSD results for the mass differential dilepton spectra in case of inclusive  $Au + Au$  collisions at  $\sqrt{s} = 200$  GeV in comparison to the data from PHENIX [18, 19] in the ‘free’ scenario, the ‘collisional broadening’ picture as well as the ‘dropping mass + collisional broadening’ model.

Fig. 2. The short dashes (black) line shows the on-shell, i.e. the standard perturbative result. The other lines show the off-shell cross section, in which the annihilating quark and antiquark have finite masses  $m_1$  and  $m_2$  with different values:  $m_1 = 0.3$  GeV,  $m_2 = 0.15$  GeV (solid magenta line),  $m_1 = 0.3$  GeV,  $m_2 = 0.3$  GeV (dash-dotted red line),  $m_1 = 0.3$  GeV,  $m_2 = 0.6$  GeV (dashed blue line),  $m_1 = 0.6$  GeV,  $m_2 = 0.6$  GeV (dash-dot-dot green line).

## 2. Comparison to data

By employing the HSD approach to the low mass dilepton production in relativistic heavy-ion collisions, it was shown in [11] that the NA60 Collaboration data for the invariant mass spectra for  $\mu^+ \mu^-$  pairs from In+In collisions at 158 A·GeV favored the ‘melting  $\rho$ ’ scenario [12]. On the other hand, the dilepton spectrum from In+In collisions at 158 A·GeV for  $M > 1$  GeV could not be accounted for by the known hadronic sources (see Fig.2 of [11]). Also, hadronic models do not reproduce the softening of the  $m_T$  distribution of dileptons at  $M > 1$  GeV [12].

In Refs. [13, 14, 15] we presented PHSD results for the dilepton spectrum as produced in  $In + In$  reactions at 158 AGeV compared to the NA60 data [12, 16]. We confirmed the HSD results that the spectrum at invariant masses below 1 GeV was better reproduced by the  $\rho$  meson yield, if a broadening of the meson spectral function in the medium was assumed. On the other hand, the spectrum at  $M > 1$  GeV was shown to be dominated by the partonic sources. Moreover, accounting for partonic dilepton sources allowed to reproduce in PHSD the effective temperature of the dileptons (slope parameters) in the intermediate mass range. The softening of the transverse mass spectrum with growing invariant mass implies that the partonic channels occur dominantly before the collective radial flow has developed.

The PHENIX Collaboration has presented dilepton data from  $pp$  and  $Au + Au$  collisions at Relativistic-Heavy-Ion-Collider (RHIC) energies of  $\sqrt{s}=200$  GeV [17, 18, 19], which show a large enhancement in  $Au + Au$  reactions (relative to scaled  $pp$  collisions) in the invariant mass regime from 0.15 to 0.6 GeV/ $c^2$ . Moreover, if realistic partial loss of the  $D$ - and  $\bar{D}$ -meson correlations due to their rescattering is kept in mind, one has to conclude that there exists another domain

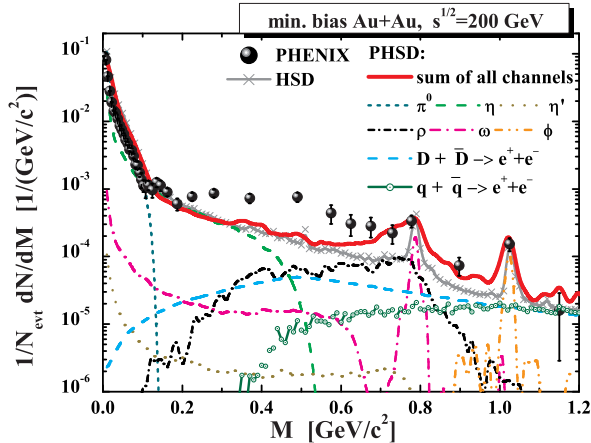


**Figure 4.** The PHSD results for the mass differential dilepton spectra in case of inclusive  $Au + Au$  collisions at  $\sqrt{s} = 200$  GeV in comparison to the data from PHENIX [18, 19] in the low mass region ( $M=0-1.2$  GeV).

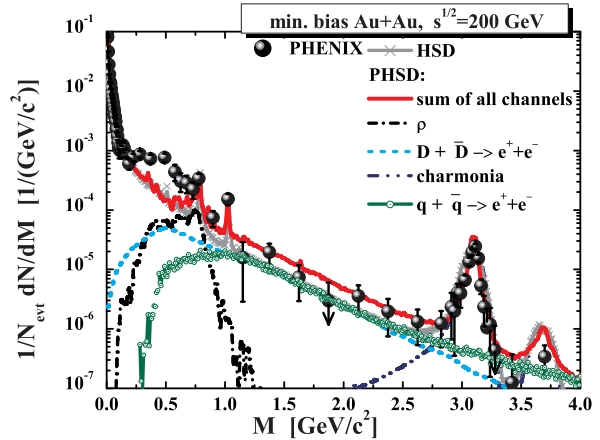


**Figure 5.** The PHSD results for the mass differential dilepton spectra in case of inclusive  $Au + Au$  collisions at  $\sqrt{s} = 200$  GeV in comparison to the data from PHENIX [18, 19] for  $M=0-4$  GeV.

of invariant mass, in which the measured dilepton yield in  $A + A$  collisions is underestimated by the scaled yield from  $p + p$ ; this domain is at masses from 1 to 4  $\text{GeV}/c^2$  [14, 20].

Let us first present in Fig 3 the HSD results for  $e^+e^-$  pairs in inclusive  $Au + Au$  collisions in comparison to the data from PHENIX [18, 19] as calculated in [11], recalling that HSD provides a reasonable description of hadron production in  $Au + Au$  collisions at  $\sqrt{s} = 200$  GeV [21]. Whereas the total yield is quite well described in the region of the pion Dalitz decay as well as around the  $\omega$ ,  $\phi$  and  $J/\Psi$  mass, HSD clearly underestimates the measured spectra in the regime from 0.2 to 0.6 GeV by approximately a factor of 5 [11]. After including the in-medium modification scenarios for the vector mesons, we achieve a sum spectrum which is only slightly enhanced compared to the 'free' scenario (see Fig. 5). The low mass dilepton spectra from  $Au + Au$  collisions at RHIC (from the PHENIX Collaboration) are clearly underestimated in the invariant mass range from 0.2 to 0.6 GeV in the 'collisional broadening' scenario as well as in the 'dropping mass + collisional broadening' model. We mention that HSD results for the low mass dileptons are very close to the calculated spectra from van Hees and Rapp as well as Dusling and Zahed [22] (cf. the comparison in Ref. [19, 23]). At higher masses (from 1 to 4 GeV) the only hadronic sources of correlated lepton pairs are the charmed mesons: semi-leptonic decays of correlated D-mesons and the dilepton decays of charmonia. Between the  $\phi$  and  $J/\Psi$  peaks, the HSD results underestimate the PHENIX data by approximately a factor of two.

By implementing the off-shell partonic processes into the PHSD transport approach, we calculate the dilepton spectra in  $Au + Au$  at  $\sqrt{s}=200$  GeV and compare to the PHENIX data in Figs. 4 and 5. In Fig. 4 we show our results for low masses ( $M = 0 - 1.2$  GeV); in this region, the yield in PHSD is dominated by hadronic sources and essentially coincides with the HSD result. Note that the collisional broadening scenario for the modification of the  $\rho$ -meson was used in the calculations presented in the Figs. 4 and 5. There is a discrepancy between the PHSD calculations and the data in the region of masses from 0.2 to 0.6 GeV. The discrepancy is not amended by accounting for the radiation from the QGP, since the latter is 'over-shone' by the radiation from hadrons integrated over the evolution of the collision. In contrast, the partonic radiation is considerable in the mass region  $M = 1 - 4$  GeV as seen in Fig. 5. The dileptons generated by the quark-antiquark annihilation in the sQGP constitute about half of

the observed yield in the mass range between the masses of the  $\phi$  and the  $J/\Psi$  mesons. For  $M > 2.5$  GeV the partonic yield dominates over the D-meson contribution. Thus, accounting for partonic radiation in PHSD fills up the gap between the hadronic model results [11, 20] and the data at  $M > 1$  GeV.

### 3. Summary

The Parton Hadron String Dynamics [1] (PHSD) transport approach incorporates the relevant off-shell dynamics of the vector mesons as well as the explicit partonic phase in the early hot and dense reaction region. A comparison of the transport calculations to the data of the NA60 Collaborations points towards a ‘melting’ of the  $\rho$ -meson at high densities, i.e. a broadening of the vector meson’s spectral function. On the other hand, the spectrum for  $M > 1$  GeV is shown to be dominated by the partonic sources.

The low mass dilepton spectra from  $Au + Au$  collisions at RHIC (from the PHENIX Collaboration) are clearly underestimated by the hadronic channels in the invariant mass range from 0.2 to 0.6 GeV. The discrepancy is not amended by accounting for the radiation from the QGP, since the latter is ‘over-shone’ by the radiation from hadrons integrated over the evolution of the collision. In contrast, the partonic radiation is visible in the mass region  $M = 1 - 4$  GeV. The dileptons generated by the quark-antiquark annihilation in the sQGP constitute about half of the observed yield in the mass range between the masses of the  $\phi$  and the  $J/\Psi$  mesons. For  $M > 2.5$  GeV the partonic yield dominates over the D-meson contribution. Thus, accounting for partonic radiation in PHSD fills up the gap between the hadronic model results and the data for  $M > 1$  GeV.

Work supported in part by the HIC for FAIR framework of the LOEWE program and by DFG. We acknowledge stimulating discussions with S. Damjanovic, V. Konchakovski and A. Toia.

### References

- [1] W. Cassing and E. L. Bratkovskaya, *Phys. Rev. C* **78** (2008) 034919, *Nucl. Phys. A* **831** (2009) 215.
- [2] W. Cassing, E. L. Bratkovskaya, *Phys. Rept.* **308** (1999) 65.
- [3] E. L. Bratkovskaya, W. Cassing, *Nucl. Phys. A* **619** (1997) 413.
- [4] W. Ehehalt, W. Cassing, *Nucl. Phys. A* **602** (1996) 449.
- [5] W. Cassing, S. Juchem, *Nucl. Phys. A* **665** (2000) 377; *ibid.* **A 672** (2000) 417.
- [6] E. L. Bratkovskaya, W. Cassing, *Nucl. Phys. A* **807** (2008) 214.
- [7] W. Cassing, *Eur. Phys. J. ST* **168** (2009) 3
- [8] L. P. Kadanoff and G. Baym, *Quantum statistical mechanics*, Benjamin, New York, 1962; C. Greiner and S. Leupold, *Ann. Phys.* **270** (1998) 328; W. Botermans, R. Malfliet, *Phys. Rept.* **198** (1990) 207; S. Leupold, *Nucl. Phys. A* **672** (2000) 475; *Nucl. Phys. A* **695** (2001) 377; Yu. B. Ivanov et al., *Phys. Atom. Nucl.* **66** (2003) 1902
- [9] V.P. Konchakovski, *PhD thesis*, University Frankfurt am Main (2009)
- [10] O. Linnyk, *J. Phys. G* **38** (2011) 025105
- [11] E. L. Bratkovskaya, W. Cassing and O. Linnyk, *Phys. Lett. B* **670** (2009) 428.
- [12] R. Arnaldi et al., NA60 Collaboration, *Phys. Rev. Lett.* **96** (2006) 162302; J. Seixas et al., *J. Phys. G* **34** (2007) S1023; S. Damjanovic et al., *Nucl. Phys. A* **783** (2007) 327c.
- [13] O. Linnyk, E. L. Bratkovskaya and W. Cassing, *Nucl. Phys. A* **830** (2009) 491C.
- [14] O. Linnyk, E. L. Bratkovskaya and W. Cassing, *AIP Conf. Proc.* **1257**, 700 (2010).
- [15] O. Linnyk, W. Cassing, E. L. Bratkovskaya and J. Manninen, arXiv:1012.0252 [nucl-th].
- [16] R. Arnaldi et al., NA60 Collaboration, *Eur. Phys. J. C* **59** (2009) 607
- [17] A. Adare et al., PHENIX Collaboration, *Phys. Lett. B* **670** (2009) 313
- [18] A. Toia et al., PHENIX Collaboration, *Nucl. Phys. A* **774** (2006) 743; *Eur. Phys. J* **49** (2007) 243; S. Afanasiev et al., PHENIX Collaboration, arXiv:0706.3034 [nucl-ex]
- [19] A. Adare et al., PHENIX Collaboration, *Phys. Rev. C* **81** (2010) 034911.
- [20] J. Manninen, E. L. Bratkovskaya, W. Cassing and O. Linnyk, arXiv:1005.0500 [nucl-th].
- [21] E. L. Bratkovskaya, W. Cassing, H. Stöcker, *Phys. Rev. C* **67** (2003) 054905; E. L. Bratkovskaya et al. *Phys. Rev. C* **69** (2004) 054907.
- [22] K. Dusling and I. Zahed, *Nucl. Phys. A* **825** (2009) 212.
- [23] A. Toia, *J. Phys. G* **35** (2008) 104037.